Mechanism and Machine Theory 164 (2021) 104397

Contents lists available at ScienceDirect

Mechanism and Machine Theory

journal homepage: www.elsevier.com/locate/mechmachtheory

Research paper

Analysis of planar compliant mechanisms based on non-linear analytical modeling including shear and lateral contraction

Stefan Henning*, Lena Zentner

Compliant Systems Group, Department of Mechanical Engineering, Technische Universitt Ilmenau, P.O. Box 100565, Ilmenau 98684, Germany

ARTICLE INFO

Article history:
Received 19 March 2021
Revised 6 May 2021
Accepted 7 May 2021
Available online 3 June 2021

Keywords:
Compliant mechanism
Flexure hinge
Analytical model
Large deflection
Software
Design tool

ABSTRACT

Compliant mechanisms are commonly used in precision engineering while analyzing their deflection is particularly challenging. Often, FEM simulations are chosen in an iterative process. Analytical approaches that consider pure bending, shear or other effects are usually limited to the mechanism as a system. However, certain configurations comprise compliant elements with different aspect ratios. The aim of this paper is to integrate the theories of shear and lateral contraction into a unified form with the existing theory of bending for large deflections and make them applicable individually for specific sections of continuous compliant mechanisms. Recommendations are made as to when which theory should be used. Building on that, a comprehensive tool for analyzing compliant mechanisms developed in Python is introduced. The tool offers the possibility to create arbitrary compliant mechanisms including branched links and various boundary conditions. A tool for parametric studies allows to optimize the given geometry for realizing a specific motion task. Further, FEM and measurement results correlate well with the application results. The presented user interface can be beneficial for the accelerated analysis and synthesis of compliant mechanisms.

1. Introduction

Due to their advantages of clearance-free and frictionless motion, scalability or high reproducibility, compliant mechanisms are applied in many engineering fields like precision engineering, micromechanics or measurement technology [1]. Typically, they represent a monolithic body with either concentrated or distributed compliance or a combination between the two [2]. The term concentrated compliance is used when the maximum dimension of a compliant segment is at least ten times smaller than the maximum length in the direction of a compliance distribution [2]. Compliant mechanisms usually achieve their motion by elastic deformation of its compliant segments. Considering concentrated compliance, mostly notch flexure hinges with different contours are applied [3]. Some of the most common ones include the circular contour [4], the corner-filleted contour [5] or the elliptical contour [6]. Each contour can provide certain advantages like a high precision but can also provide drawbacks like large elastic strain concentrations. A good compromise between the two is achieved with

* Corresponding author.
E-mail addresses: stefan.henning@tu-ilmenau.de (S. Henning), lena.zentner@tu-ilmenau.de (L. Zentner).
URL: http://www.tu-ilmenau.de/en/nsys (S. Henning)

https://doi.org/10.1016/j.mechmachtheory.2021.104397

the power function-based flexure hinge contour [7]. Its compliance distribution is largely influenced by the adjustment of the exponent of the power function.

Because of the monolithic design of compliant mechanisms and geometric non-linearity occurring as a result of large deflections, the analysis of important elasto-kinematic properties and the motion behavior under given loads or displacements is non-trivial.

It is widely accepted that the most accurate results may be achieved by simulations using finite elements method (FEM) [8]. However, those need to be distinguished between the number of possible deformation directions that are defined by different element types and by the possible degrees of freedom for the overall model (1D/2D/3D). More specifically, the higher the number of possible deformation directions of the finite element and the higher the possible degrees of freedom, the more accurate a solution can be for the whole model. Hence, 3D solid elements provide results closest to reality. Beam elements, i.e. 1D/2D FEM can be a valuable tool for the compliant mechanism design due to fast calculation times [9]. However, certain 3D effects like lateral contraction are neglected but may be important for specific aspect ratios. Large deflections, non-linear material properties, shear, lateral contraction, axial elongation or 3D effects like stress concentration [10,11] or anticlastic bending [12] can be considered even for seemingly planar motions. Also, 3D mechanisms and out of plane loads and deformations can be modeled. Nonetheless, the accuracy largely depends on the discretization, the element type and the degrees of freedom (1D/2D/3D). Calculation times are typically compromised by a higher discretization.

Apart from FEM simulations, a number of different methods exist for the flexure hinge and compliant mechanism analysis and synthesis. Overviews are given in [13] and in [14]. When large deflections are considered, an analytical description of the deformed state usually leads to a system of differential equations in the form of a boundary value problem (BVP). Because of this, approximate approaches like design equations (DE) derived by empirical data obtained with FEM or analytical models can be chosen (e.g. [4,6,15,16]). Rarely, closed form equations are proposed for large deflections [15]. There are several benefits for using DE like the explicit form that enables the usage without special tools and application without experience. Also, results are obtained very fast which is why those are suitable for synthesis. Despite the advantages, most DE are only approximations specific to certain geometries and may only be valid within ranges for specific aspect ratios. Apart from this, they are usually not available for complex mechanisms.

To calculate compliant mechanisms, the rigid-body model (RB) (e.g. [1,15,17–20]) has won recognition for its simplicity. The model is based on the principle to replace the compliant mechanism by rigid links and conventional hinges connected to each other by torsion and/or linear springs. Different RB exist in literature with varying degrees of accuracy. Advantages are the simple formulation and applicability to complex mechanisms as well as the consideration of large deflections and good agreement with non-linear beam theory [21]. However, the accuracy largely depends on the discretization and a rise in degrees of freedom can drive up computation time. RBs are also mostly load-dependent and may need a second ”design step” to assess a final CM configuration. Besides, the position of the conventional hinges in the RB depends on the type of the compliant element. This results in an error in the deflection, since the displacement of the axis of rotation is not taken into account. Further, it has been shown that a considerable amount of deformation also occurs within the links and the frame of a compliant mechanism [22,23].

Other approaches are based on kinetostatic analysis for obtaining the deformation behavior of compliant mechanisms. Those can for example be based on a compliance matrix approach [19,24]. With this method, the displacements at one point of a rigid link and the load on that link are related to the deformations at the end point of a flexure hinge. Advantages are the simple formulation, simultaneous consideration of axial elongation, shear and bending whereas the method is only valid for small deflections. Further approaches are applying energy based models (EM) for the kinetostatic analysis like virtual work principles [21,25,26]. In summary, the equilibrium position of a compliant mechanism is achieved by determining the minimum potential energy state of the mechanism so that the structural integrity is maintained. Virtual work refers to both, the work done by a force on a system during a virtual displacement and the work done by a virtual force on a real displacement. This principle is used to calculate the equilibrium in the overall system. Applied to a continuum, it does not provide the complete deformation state of the overall system but only forces, angles or displacements at defined points.

Another popular model is the chained beam constraint model (CBCM) (e.g. [27,28]) and can be applied to beam-based compliant mechanisms. In the CBCM model, individual beams are discretized into a number of elements that are chained together. The shape of the beams is defined by geometric constraints. Various boundary conditions and load cases can be considered. With the model, a solution can be provided in an explicit form for a given mechanism which enables an efficient calculation process. Therefore, once the CBCM has been obtained, it is suitable for synthesis by optimizing geometric parameters. By discretizing using circular arc elements or similar, even initially curved beams can be calculated [29]. The model is also available for the consideration of shear [27]. The authors see the main limitation of this method in the fact that the accuracy of the solution depends strongly on the discretization. Furthermore, in the opinion of the authors, the method is only suitable to a limited extent for the implementation in software applications for the analysis of arbitrary planar mechanisms, since the model is valid for only one particular geometry and must first be derived anew for other mechanisms.

A well-known analytical approach for calculating compliant mechanisms or flexure hinges is the non-linear beam theory (BT) also referred to by the theory for large deflections of rod-like structures [2]. It has previously been shown, that the theory can be applied to complex compliant mechanisms due to the continuous approach [30]. Advantages of the method include the consideration of large deflections and the possibility for modeling non-constant cross-sections, curvatures and material properties. There is a certain versatility to the model because arbitrary boundary conditions or even contacts,

Table 1
Overview of existing applications for the flexure hinge and compliant mechanism design – The * indicates that the software is available for download or online usage, FH: flexure hinge, CM: compliant mechanism, con.: concentrated, dist.: distributed, An.: analysis, Syn.: synthesis, DE: design equations, PR: pseudo rigid-body model, EM: energy method, FE: finite elements method, BT: beam theory, TO: topology optimization, S: shear, PS: plane strain, AE: axial elongation, LD: large deflections (geometric non-linearity), DL: deformable links, CS: contour-specific modeling, BL: branched links.

ref.	subject	dim.	comp.		applic.		model						effects			considering			
			con.	dist.	An.	Syn.	DE	PR	EM	FE	BT	TO	S	PS	AE	LD	DL	CS	BL
V[a]*	FH	2D	x		x		x											x	
J[b]*	FH/CM	2D	x	x	x		x										x		
[18]	CM	2D/3D	x	x	x	x		x	x				x	x		x		x	x
[19]	CM	2D/3D		x	x	x					x						x	x	x
[21]*	CM	2D		x	x	x		x	x							x			x
[31]*	FH	2D	x		x		x											x	
[32]	FH	2D	x		x						x		x			x		x	
[33]*	FH	2D	x	x	x						x					x	x	x	
[34]	CM	2D/3D		x	x	x		x					x			x			
[35]	CM	2D		x		x						x				x	x		x
F[c]	CM	2D		x		x						x					x		x
[36]*	CM	2D/3D		x		x						x	x		x		x		x
S[d]*	CM	2D/3D	x	x	x					x			x		x	x	x		
C[e]*	FH/CM	2D	x	x	x	x					x		x	x		x	x	x	x

[a] *Vink System Design & Analysis*
[b] *Janssen Precision Engineering (JPE)*
[c] *FlexWorks*™
[d] *SPACAR*
[e] *CoMUI* – subject of this paper

branching points and arbitrary load cases by (distributed) forces or moments can be assumed. Also, shear and lateral contraction can be implemented into the model. Because of the continuity, a compliant mechanism can be subdivided into several sections. This leads to the opportunity of applying different theories specifically to individual sections of a mechanism. Hence, sections with different aspect ratios can be modeled accordingly. In addition to this, the model is scalable when considered dimensionless. The BVP can be solved fast and accurate by modern solvers. Therefore, it is also suitable for parametric studies and synthesis and highly suitable for the implementation in graphical software tools. Apart from this, the theory exists for 2D and 3D scenarios. In contrast, the individual implementation for specific mechanisms can be complicated. Also, mathematical expressions for cross-sections, curvatures or the YOUNGS modulus need to be obtained for each mechanism. Not only may the efficiency and accuracy of the applied BVP-solver largely depend on tolerances for the solution but also on initial guesses.

The number of benefits from modeling compliant mechanisms utilizing BT and the limits of other modeling techniques are the foundation of the approach described in this paper. Some of the mentioned models can include the effects of shear, lateral contraction or axial elongation. Usually, those models are applied for the whole mechanism. However, compliant mechanisms can include different elements of concentrated and distributed compliance with varying aspect ratios. These may require different effects to be considered. The authors do not know of any analytical approach that allows for the individual consideration of those effects for specific sections of a compliant mechanism. The goal in this paper is to present the different theories (pure bending, shear and lateral contraction) in a unified form and to make them applicable individually or in combination for specific sections of a compliant mechanism using BT. Recommendations are given as to when to use which theory.

Despite the large number of models and techniques, the applicability for an engineer with little experience in the design of compliant mechanisms may be limited due to a lack of simplified tools available. Building on the different theories mentioned, a graphical user interface is developed as a secondary goal of this paper, further referred to as *CoMUI*, that enables the element-wise selection of the three different theories.

In literature, there are very few, tangible or accessible tools to model and analyze mechanisms in a targeted manner, which is why time-consuming 3D FEM is often used. An overview of the design and calculation tools known to the authors is shown in Table 1.

Some of these tools consist of an intuitive graphical user interface that runs without additional software (e.g. *Vink System Design & Analysis*) or web-based calculators for single flexure hinges [31]. Furthermore, calculation scripts for flexure hinges (FH) and specific compliant mechanisms (CM) based on *Mathcad*® are available on the website of *Janssen Precision Engineering* (*JPE*). Their calculations are based on approximate design equations from [37]. Also, software scripts for *MATLAB*® are available, e.g. [36]. Many of the tools are focused on the synthesis of compliant mechanisms. These are often based on the pseudo rigid-body model alone [18,21,34] or on topology optimization utilizing genetic algorithms [35], finite elements method [36], pseudo rigid-body models [38] or the chained beam constraint model [28]. With regard to topology optimization, a great overview of educational computer tools is given in [39]. In addition, there is a software called *FlexWorks*™ from the company *FlexSys Inc.* founded by Dr. Sridhar Kota that suggests a topology based on a required in- and output motion. Many of the available tools for the analysis of compliant elements are only subject to specific flexure hinge contours (e.g. *V*[1],

J^2, [31–33]) or pre-designed compliant mechanisms (e.g. J^2,) while others offer more design possibilities (e.g. [18,19,21,34], S^4). In eight of the thirteen applications found, pure bending is assumed in the respective model. Other ones include the effects of shear (S), lateral contraction (PS) or axial elongation (AE) in their models. Besides, for about half of the applications in Table 1, large deflections (LD) are considered. In seven applications not only the compliant elements but also the links of a mechanism are considered deformable (DL) which is important in precision engineering. Six of the total applications enable the contour-specific design (CS) of flexure hinges. Apart from this, in about half of the applications, branched links (BL) are taken into account. Nevertheless, an extensive tool that implies all of the mentioned features combined into a single application is not known to the authors.

Hence, in this paper a software tool containing the given analytical approach is presented that enables an intuitive design, analysis and synthesis of compliant mechanisms. Based on the state-of-the-art modeling techniques for compliant mechanisms and the available applications for the flexure hinge and compliant mechanism design in Table 1, the following aspects are highlighted that should be addressed with the developed software *CoMUI*.

- One drawback for some of the tools in Table 1 may be the limited graphical user interfaces. Therefore, the goal for *CoMUI* is to provide an extensive interface for the intuitive and quick design of compliant mechanisms, an efficient analysis and a simple way to modify them.
- As outlined, the deformation of the links between hinges is often neglected in many applications. In *CoMUI*, compliant mechanisms are described as continua to include those deformations.
- Some of the previous tools may be limited to simple geometries. With the given model, arbitrary geometries can be considered. This includes flexure hinges with cut-out geometries of any given form and curved beams.
- In some of the above-mentioned tools, only small deflections are considered which may limit an accurate analysis. For instance, compliant mechanisms with straight-line deformations may deviate in parasitic directions. Those deviations are only covered, when large deflections are considered.
- Most of the tools are either limited to concentrated or distributed compliance. Certain compliant mechanisms can require a combination of the two which is why with *CoMUI* it is possible to incorporate both.
- The analysis and synthesis of compliant mechanisms often relies on commercial computer-aided design (CAD) frameworks. In contrast, *CoMUI* is developed using the free and open source programming language *Python*.
- Some of the tools in Table 1 consider shear, lateral contraction or axial elongation for the whole mechanism. In *CoMUI* individual effects can be applied section-wise for the distinction between varying aspect ratios.

In summary, due to the computing performance of modern numerical calculation software, the deformed state of a compliant mechanism can be calculated within fractions of a second using beam theory. The modeling legitimates both concentrated and distributed compliance, straight and curved segments as well as non-constant cross-sections, curvatures or variable material properties. Due to the efficiency of the analytical model and the adaptability to arbitrary plane mechanisms, the solution approach is particularly suitable for the implementation in a software application. Nevertheless, the consideration of pure bending is insufficient for certain applications, because it is possible to deviate from Bernoulli's hypotheses if arbitrary geometry specifications can be made. In Section 2, first pure bending is considered in the analytical model. Subsequently, in addition to bending, the influence of shear under large deflections is included and novel differential equations are formulated to put the theory into the same form as the given beam theory. Afterwards the effect of lateral contraction is taken into account, too. The new approach allows to shift the limits of the previous model, so that beyond thin beams also geometries with a larger height to length or width to length ratio can be considered. Because of the unified equations for all three theories and the beams continuity, those theories can be applied for different sections of the mechanism individually. In Section 3, an implementation of the derived models into a graphical user interface, based on *Python* is demonstrated. Finally, results obtained with the software application are verified by FEM simulation and measurement results from previous studies. Also, further mechanism examples and use cases of the software are shown.

2. Analytical approach

The analytical model is based on the theory for large deflections of rod-like structures [2] because of its versatility for describing arbitrary shaped and oriented compliant mechanisms in plane. It has been applied to compliant mechanisms by the authors before, for example in [30] with great accordance compared to FEM simulations and measurements. In literature, rod-like structures are defined as beams whose cross-sectional dimensions are at least ten times smaller than their length or curvature radii [2]. Due to those limitations, previous investigations were focused on pure bending. With this paper, the authors aim to include the effects of shear and lateral contraction for considering a wider range of possible geometries beyond those limits.

2.1. Theory for large deflections of rod-like structures

The mathematical model is derived from the deflected state of a single beam with a Young's modulus E, a length L, a width w and a height H under the two direction-constant external forces and the external moment in Eq. 1. Only direction-constant and no follower forces are considered because compliant mechanisms are mostly actuated by linear actuators, e.g.

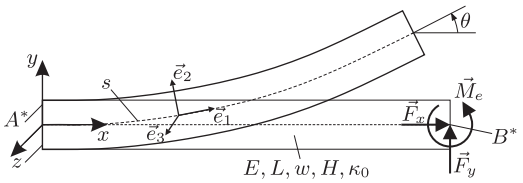

Fig. 1. Beam in its undeflected and deflected state loaded with two external direction-constant forces $\vec{F}_x$ and $\vec{F}_y$ as well as an external moment $\vec{M}_e$.

[40].

$$\vec{F}_x = F_x\vec{e}_x,\ \vec{F}_y = F_y\vec{e}_y,\ \vec{M}_e = M_e\vec{e}_z \tag{1}$$

The beam shown in Fig. 1 is fixed at point A^* and loaded at the free end at point B^* resulting in the deflected state due to the consideration of large deflections. The beam axis s is introduced in the deformed state. The validity of Hooke's law, Saint-Venant's principle and Bernoulli's hypotheses are assumed. Due to the consideration of pure bending, the cross-sections are perpendicular to the beam axis. A deflection angle θ results. The following system of differential equations is obtained:

$$\frac{\mathrm{d}M_z}{\mathrm{d}s} = F_x\sin\theta - F_y\cos\theta, \tag{2}$$

$$\frac{\mathrm{d}\theta}{\mathrm{d}s} = \kappa,\ \text{with}\ \kappa = \frac{M_z}{EI_z} + \kappa_0, \tag{3}$$

$$\frac{\mathrm{d}x}{\mathrm{d}s} = \cos\theta, \tag{4}$$

$$\frac{\mathrm{d}y}{\mathrm{d}s} = \sin\theta. \tag{5}$$

Therein, M_z represents the resulting bending moment, κ_0 represents the curvature in the undeformed state, κ represents the curvature in the deformed state and I_z represents the second moment of inertia. The boundary conditions for the example in Fig. 1 are as follows:

$$M(L) = M_e,\ \theta(0) = 0,\ x(0) = 0,\ y(0) = 0. \tag{6}$$

With regard to the Eqs. 2–6, it should be noted that both forces F_x and F_y, the moment M_e, the curvature in the undeformed state $\kappa_0 = \kappa_0(s)$, the Young's modulus $E = E(s)$ and the second moment of inertia $I_z = I_z(s)$ represent parameters or functions specific to a certain application and, moreover, may vary along the path of the rod axis s, as in case of flexure hinges or curved beams.

The system consists of first order, non-linear, non-autonomous, ordinary differential equations and often cannot be solved in an explicit analytical form, especially when κ_0, E or I_z are not constant. For this reason, numerical approaches can be a suitable option for accurately approximating a solution.

A solution of the boundary value problem may be obtained numerically as described in Section 3. The boundary conditions can be changed as needed for a specific mechanism.

2.2. Considering shear

One of the main assumptions of the previous analytical model in the Eqs. 2–5 is the fact that the cross-sectional dimensions have to be at least ten times smaller than the length and the curvature radii of the beam [2] so that the consideration of pure bending is sufficient for obtaining accurate results.

In contrast, shorter beams that experience a considerable amount of deflection cannot be accurately calculated using pure bending. In that case, unlike the previous model it should not be assumed that the cross-sections remain perpendicular to the beam axis. Because of this, the additional deformation in the form of shear will be considered. The original considerations of shear date back to the works of Prof. Timoshenko who considered shear deformation for small deflections [41]. Following, the effects of shear will be applied in the form of differential equations to be implemented into the existing theory for large deflections of rod-like structures.

Allowing additional beam deformation due to shear reduces the stiffness of the beam compared to calculations using Bernoulli's hypotheses. Therefore, higher deformations can be expected. In order to incorporate the deformation due to shear, pure shear without bending is considered first. Fig. 2 (a) is used for illustration.

A shear angle gamma indicates the angle between the normal of the beam axis and the cross-section in the deformed state. In contrast to normal stresses, shear stresses cannot be assumed as constant over the cross-sectional area. The shear

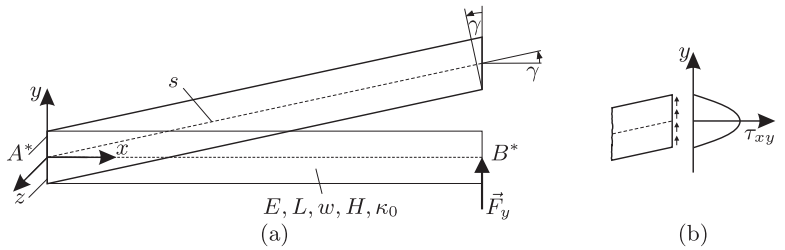

Fig. 2. Deformation of a beam considering pure shear deformation – (a) beam in its undeflected and deflected state loaded with an external direction-constant force $\vec{F}_y$, (b) shear stress distribution in the cross-section.

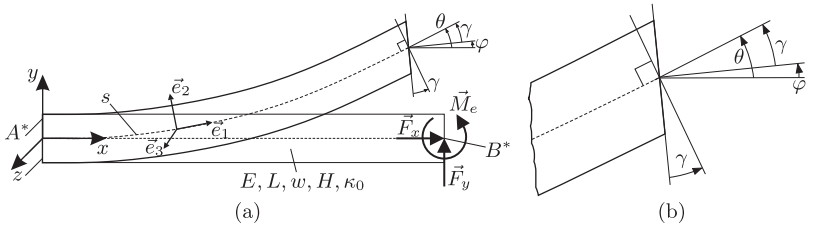

Fig. 3. Deformation of a beam overlaying shear and bending deformation – (a) beam in its undeflected and deflected state loaded with two external direction-constant forces $\vec{F}_x$ and $\vec{F}_y$ as well as an external moment $\vec{M}_e$, (b) magnification of the beams end.

stresses at the boundary of the cross section are zero. In Fig. 2 (b) it is shown that the greatest shear stress occurs at the beam axis. A correction is applied to the effective shear area $A_s = \varkappa A$ as a reduction of the cross-sectional area A of a beam using a correction factor $\varkappa$. This factor is derived from the condition "that the strain energies of the real and of the averaged shear stress state generated during deformation are equal" [42]. For example, $\varkappa = \frac{5}{6}$ applies to a rectangular cross-section [42]. The shear stress equation as a result of a shear force $Q_s(s)$ in the beams cross-section is:

$$\tau(s) = \frac{Q_s(s)}{A_s(s)} = \frac{Q_s(s)}{\varkappa A(s)}. \tag{7}$$

From Hooke's law a relation between shear stress and shear strain with the help of the shear modulus G follows. The shear modulus G describes the ratio between the shear stress τ and the shear angle γ:

$$\tau = G\gamma. \tag{8}$$

The connection of equation Eq. 7 and Eq. 8 results in a relation between shear force and shear angle:

$$\gamma = \frac{Q_s(s)}{\varkappa A(s) G}. \tag{9}$$

Now the beam is considered by overlaying the bending deformation with the shear deformation. The resulting deflection is shown in Fig. 3 (a) and magnified in Fig. 3 (b). This shows which angles are of special importance. As before in the case of the theory of large deflections of rod-like structures, the angle of the beam axis is called θ.

An angle φ is introduced between the x-axis and the normal of the deformed cross-sectional area. Likewise, the shear angle between the cross-section normal in the deformed state and the beam axis tangent can be found again. Consequently, a relation of the three angles can be formulated:

$$\theta = \varphi + \gamma. \tag{10}$$

For the unloaded state Eq. 11 results analogously.

$$\theta_0 = \varphi_0 + \gamma_0 \tag{11}$$

Since there is no shear force in the unloaded state, $\gamma_0 = 0$ and $\frac{\mathrm{d}\gamma_0}{\mathrm{d}s} = 0$ follows. The curvature of the beam axis is defined as the derivative of the angle θ. For the unloaded state Eq. 12 follows.

$$\kappa_0 = \frac{\mathrm{d}\theta_0}{\mathrm{d}s} = \frac{\mathrm{d}\varphi_0}{\mathrm{d}s} \tag{12}$$

Next, to incorporate the material properties, the deformation equations are derived analogous to [2] from the strain ε_1 of a beam fiber. The axial elongation is regarded as the change in length of the fiber $\mathrm{d}s_f$ when deformed. This fiber is distanced from the neutral fiber $\mathrm{d}s$ by the coordinate r_2 within the cross-section in the loaded state. Its length before the deformation is given as $\mathrm{d}s_{f0}$. Fig. 4 serves as an illustration.

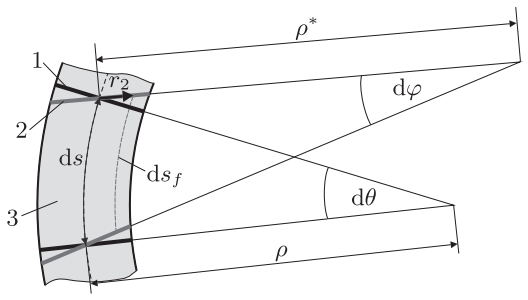

Fig. 4. Deformed state of a beam segment considering shear – 1: cross-section being orthogonal to the beam axis, 2: cross-section that has been orthogonal to the beam axis in the unloaded state, 3: beam element containing an element of length ds.

The strain is obtained as follows:

$$\varepsilon_1 = \frac{\mathrm{d}s_f - \mathrm{d}s_{f0}}{\mathrm{d}s_{f0}} = \frac{(\rho^* - r_2)\mathrm{d}\varphi - (\rho_0 - r_{20})\mathrm{d}\theta_0}{(\rho_0 - r_{20})\mathrm{d}\theta_0}. \tag{13}$$

Therein ρ is the curvature radius of the beam axis and ρ^* the radius of the arc dφ. Furthermore, ρ_0 reflects the curvature radius in the unloaded state and r_{20} the coordinate of the fiber ds_f in the cross-section of the undeformed state (not shown). It should be noted that r_{20} and r_2 remain equal. The length of the beam axis remains constant, so the following applies:

$$\rho_0 \mathrm{d}\theta_0 = \rho \mathrm{d}\theta \tag{14}$$

From the geometric relationship Fig. 4 the following relationship can be formulated for ds:

$$\mathrm{d}s = \rho_0 \mathrm{d}\theta_0 = \rho \mathrm{d}\theta = \rho^* \mathrm{d}\varphi. \tag{15}$$

This results in:

$$\frac{\mathrm{d}\varphi}{\mathrm{d}\theta_0} = \frac{\rho_0}{\rho^*}. \tag{16}$$

With Eq. 16 it follows from Eq. 13 that:

$$\varepsilon_1 = \frac{\rho_0(\rho^* - r_2) - \rho^*(\rho_0 - r_2)}{\rho^*(\rho_0 - r_2)}. \tag{17}$$

A simplification leads to:

$$\varepsilon_1 = \frac{r_2}{\rho_0 - r_2} \cdot \frac{\rho^* - \rho_0}{\rho^*}. \tag{18}$$

Assuming that r_2 is much smaller than ρ_0, Eq. 18 results in:

$$\varepsilon_1 = r_2\left(\frac{1}{\rho_0} - \frac{1}{\rho^*}\right). \tag{19}$$

The bending moment is given in [2]:

$$M_z = \int (-r_2 \sigma_1)\mathrm{d}A \tag{20}$$

The stress is obtained by Hooke's law:

$$\sigma_1 = E\varepsilon_1. \tag{21}$$

Using the strain from Eq. 19 this yields:

$$M_z = -\int \left(r_2 E r_2\left(\frac{1}{\rho_0} - \frac{1}{\rho^*}\right)\right)\mathrm{d}A = E\left(\frac{1}{\rho^*} - \frac{1}{\rho_0}\right)\int r_2^2 \mathrm{d}A. \tag{22}$$

Then follows with the knowledge of $\int r_2^2 \mathrm{d}A = I_z$ and with the information from Eq. 12 and Eq. 15:

$$M_z = EI_z\left(\frac{1}{\rho^*} - \frac{1}{\rho_0}\right) = EI_z\left(\frac{\mathrm{d}\varphi}{\mathrm{d}s} - \kappa_0\right). \tag{23}$$

Lastly, the shear force $Q_s(s)$ for the formulation of the angle γ (Eq. 9) is needed. Because the shear force is defined in plane with the cross section of the deformed beam, Eq. 24 is obtained.

$$Q_s(s) = -F_x \sin\varphi + F_y \cos\varphi \tag{24}$$

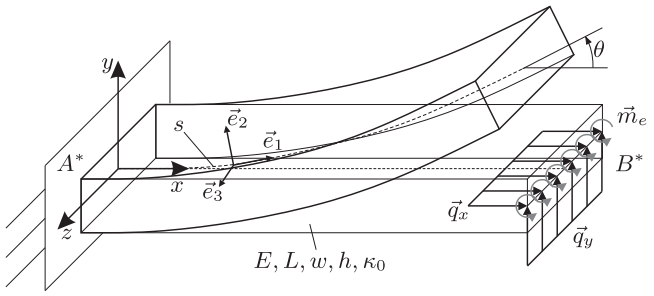

Fig. 5. Plate in its undeflected and deflected state loaded with two external direction-constant line loads $\vec{q}_x$, $\vec{q}_y$ and $\vec{m}_e$ (shown in gray).

Finally, the system of differential equations is obtained. The main difference compared to pure bending can bee seen between Eq. 3 and Eq. 26:

$$\frac{\mathrm{d}M_z}{\mathrm{d}s} = F_x \sin(\varphi + \gamma) - F_y \cos(\varphi + \gamma), \tag{25}$$

$$\frac{\mathrm{d}\varphi}{\mathrm{d}s} = \frac{M_z}{EI_z} + \kappa_0, \tag{26}$$

$$\frac{\mathrm{d}x}{\mathrm{d}s} = \cos(\varphi + \gamma), \tag{27}$$

$$\frac{\mathrm{d}y}{\mathrm{d}s} = \sin(\varphi + \gamma), \tag{28}$$

$$\text{with } \gamma = \frac{-F_x \sin\varphi + F_y \cos\varphi}{\varkappa AG}. \tag{29}$$

The boundary conditions for the example in Fig. 3 are as follows:

$$M(L) = M_e,\ \varphi(0) = 0,\ x(0) = 0,\ y(0) = 0. \tag{30}$$

2.3. Considering lateral contraction

Due to the fact that in compliant mechanism often flexure hinges are implemented that exceed a width to length ratio significantly greater than 0.1, a further discrepancy from Bernoulli's hypothesis that is only valid for thin beams is made. It therefore seems obvious that the resulting effect of lateral contraction should be added to the equations.

Following, the system of differential equations for pure bending is extended to include those effects. Strictly speaking, these geometries are not thin beams but rather plate-like structures for which some assumptions have to be made deviating from the theory of large deflections of rod-like structures (see [43], [10]).

Up to now it was assumed that strains in the beam only occur in longitudinal direction ($\vec{e}_1$). For structures with a greater width to length ratio (Fig. 5), the development of stresses in lateral direction is also taken into account.

With a low height to length ratio deformations in $\vec{e}_2$-direction are still unhindered, but not in $\vec{e}_3$-direction due to the large width. The lateral contraction in $\vec{e}_3$-direction is hindered, that means a plane strain state results. If a beam segment is subjected to longitudinal stress σ_1 in addition to a lateral stress σ_3, the longitudinal elongation is reduced by the proportionate lateral strains (e.g. [44]). In the geometrically non-linear plate theory, the axial stress σ_1 and the strains in the $\vec{e}_3$-direction ε_3 are related in the following way, which is derived from Hooke's law:

$$\varepsilon_1 = \frac{1}{E}(\sigma_1 - \nu\sigma_3) \tag{31}$$

$$\varepsilon_3 = \frac{1}{E}(\sigma_3 - \nu\sigma_1) \tag{32}$$

Wide cross-sections require the assumption $\varepsilon_3 = 0$, so that $\sigma_3 \neq 0$ [43]. Thus, from Eq. 31 and Eq. 32 follows:

$$\varepsilon_1 = \frac{\sigma_1}{E}(1 - \nu^2). \tag{33}$$

Fig. 5 shows the deformed state of a plate. The forces $\vec{F}_x$ and $\vec{F}_y$ as well as the moment $\vec{M}_e$ at the end of the plate are constant over the width of the plate in the form of line loads $\vec{q}_x$, $\vec{q}_y$ and $\vec{m}_e$. Taking $F_x = q_x w$, $F_y = q_y w$ and $M_e = m_e w$ into account,

the system of differential equations for the hindrance of lateral contraction is formulated analogously to the Eqs. 2–5. The difference lies only in the factor $1-\nu^2$:

$$\frac{\mathrm{d}M_z}{\mathrm{d}s} = F_x \sin\theta - F_y \cos\theta, \tag{34}$$

$$\frac{\mathrm{d}\theta}{\mathrm{d}s} = \kappa, \text{ with } \kappa = \frac{M_z}{EI_z}(1-\nu^2) + \kappa_0, \tag{35}$$

$$\frac{\mathrm{d}x}{\mathrm{d}s} = \cos\theta, \tag{36}$$

$$\frac{\mathrm{d}y}{\mathrm{d}s} = \sin\theta. \tag{37}$$

The boundary conditions in this case are identical to Eq. 6.

2.4. Calculation of elasto-kinematic properties

After the system of differential equations is solved, solutions for the four equations $M_z(s)$, $\theta(s)$, $x(s)$ and $y(s)$ are available for each point along the beam axis s. Using these results, it is possible to evaluate elasto-kinematic properties such as displacements, angles and strains for each section. Displacements can be calculated using the resulting coordinates x and y in the deformed state and subtracting the specific coordinates in the undeformed state x_0 and y_0. The orientation of each point along s is given by the resulting angle θ. This result can be used to calculate hinge angles as the relative angle between the beginning and the end of a flexure hinge. Elastic strains can be calculated at $z=0$ using the bending moment $M_z(s)$ with the according maximum distance from the beam axis to the outer fiber $\eta(s)$ within the cross section:

$$|\varepsilon(s)| = \frac{|M_z(s)|}{EI_z(s)}\eta(s). \tag{38}$$

2.5. Geometric parameters and boundary conditions

In this section important geometric parameters and necessary boundary conditions for the mechanism design are presented. Because the mechanisms need to be designed as continua according to the analytical model, the beam axis of the complaint mechanisms can only contain straight or curved sections of various cross-sections and must not contain any kinks. An arbitrary but continuous compliant mechanism may be composed by using the three basic building blocks, further referred to as elements, shown in Fig. 6.

The two basic geometric parameters height H and width w apply for all three elements. The contour-specific parameters of the power function based contour are the minimum notch height h and the exponent n. Within the analytical model, the cross section of these elements is implemented by I_z which may also be $I_z(s)$ with the according height function in Eq. 39 [45] in case of the beam element with power function-based contour (Fig. 6 (c)).

$$h(s) = h + 2^n \frac{H-h}{L^n}|s|^n, \text{ with } n \in \mathbb{R},\ n > 1 \tag{39}$$

While the axial dimension for both, the beam element with constant cross-section and the element with power function-based contour is defined by the length L, the length of the curved beam element may be calculated by specifying the curvature angle α and the curvature radius ρ_0 according to Eq. 40.

$$L = \alpha\rho_0 \tag{40}$$

An arbitrary initial curvature can be implemented by a function $\kappa_0 = \kappa_0(s)$. Initial curvatures of circular shape (Fig. 6 (b)) can easily be realized with the curvature radius ρ_0:

$$\kappa_0 = \frac{1}{\rho_0}. \tag{41}$$

In summary, interconnecting an arbitrary amount and order of the three different elements and adjusting their geometry, allows to model a variety of compliant mechanisms. Each of these elements can represent a concentrated or distributed compliance, depending on the given dimensions of the mechanism. Furthermore, a combination between different elements is also possible. For example the elements in Fig. 6 (b) and (c) can be combined to obtain a curved flexure hinge. Thus, a wide range of applications can be realized.

It is also intended to provide a selection of different boundary conditions at both ends of the mechanism. This enables to model frequent applications such as slider cranks, fixed or free ends. In addition, the position and orientation of the origin of point A^* should also be variable. The selection of boundary conditions is shown in Fig. 7.

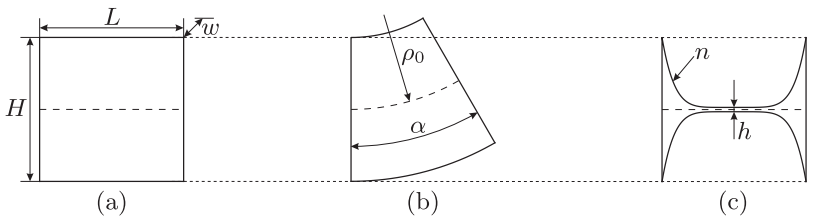

Fig. 6. Three different beam elements for designing a planar compliant mechanism – (a) beam element with constant cross-section, (b) curved beam element, (c) beam element with power-function based contour.

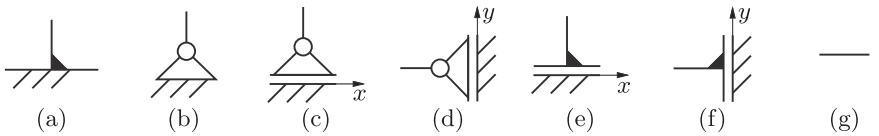

Fig. 7. Sketched representation of the considered boundary conditions – (a) fixed support, (b) hinged support, (c) hinged support with slider in x-direction, (d) hinged support with slider in y-direction, (e) slider in x-direction, (f) slider in x-direction, (g) free end.

With respect to the chosen boundary conditions in Fig. 7, no statically indeterminate systems are considered. Therefore, the support at point A^* is either considered fixed (Fig. 7 (a)) or hinged (Fig. 7 (b)). In the case of a fixed end at point A^*, the desired static determination is achieved for any selection of the boundary conditions for point B^*. In contrast, when a hinged support is chosen for point A^* the system is then statically determined, when any boundary condition except a free end is chosen at point B^*. When the boundary conditions are changed, Eq. 6 (resp. Eq. 30) has to be changed accordingly.

2.6. Modeling procedure for transitions between elements

Compliant mechanisms may contain an arbitrary combination and number of the different elements in Fig. 6. In this paper, two possible transitions between adjacent elements are considered. On one hand, the continuous transition from one element to the next (Fig. 8 (a)) and on the other hand the transition at a branching point K (Fig. 8 (b)).

The rod axis s of a random mechanism with only continuous transitions is shown in Fig. 8 (a). The mechanism consists of an arbitrary number of interconnected elements. The element at t-th position is defined by the parameters L_t, H_t, w_t, h_t, n_t, $\kappa_{0,t}$, $F_{x,t}$, $F_{y,t}$ and $M_{e,t}$. The transition conditions between the two adjacent elements t and $t+1$ at the coordinate $s = \sum_{t=1}^{t} L_t$ (point T) are:

$$M_{z,t+1} = M_{z,t} + M_{e,t},\ \theta_{t+1} = \theta_t,\ x_{t+1} = x_t,\ y_{t+1} = y_t. \tag{42}$$

Furthermore, for the consideration of branched mechanisms the approach from [30] is applied. When a branched mechanism becomes necessary, three continuous beams result that are interconnected at the branching point K. Each of those beams is described with an individual beam axis s_1, s_2 and s_3. The system of differential equations is considered for each beam individually. This means, that each of the individual beams can be comprised of an arbitrary number of elements with a continuous transition between them as described above. However, at the location of the branching point K, different transition conditions are applied. When assuming a total number of u elements for the first beam, the u-th element of the first beam, the first element of the second beam and the first element of the third beam are connected at point K, located at $s_{1\text{end}} = \sum_{t=1}^{u} L_t$, $s_2 = 0$ and $s_3 = 0$. The following transition conditions apply for the second beam:

$$\theta_2(0) = \theta_1(s_{1\text{end}}) + \theta_{20},\ x_2(0) = x_1(s_{1\text{end}}),\ y_2 = y_1(s_{1\text{end}}). \tag{43}$$

The same applies for the third beam:

$$\theta_3(0) = \theta_1(s_{1\text{end}}) + \theta_{30},\ x_3(0) = x_1(s_{1\text{end}}),\ y_3 = y_1(s_{1\text{end}}). \tag{44}$$

For branched mechanisms it is always assumed that the first beam originates at point A^* and the second beam ends at point B^* for which boundary conditions are applied (cf. Fig. 12). The end of the third beam is always considered as a free end. Introducing a branching point leads to further unknown system parameters which are compensated by an additional boundary condition for the bending moment $M_{z,3}$ at the free end of the third beam:

$$M_{z,3}(s_{3\text{end}}) = 0 \tag{45}$$

and by an additional transition condition at the branching point K:

$$M_{z,1}(s_{1\text{end}}) = M_{z,2}(0) + M_{z,3}(0). \tag{46}$$

A more detailed breakdown of boundary and transition conditions for branched mechanisms is given in [30].

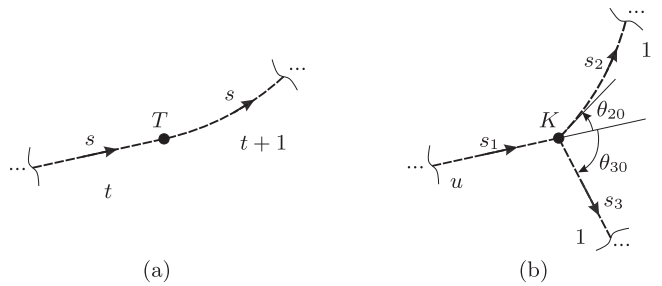

Fig. 8. Transition between adjacent links – (a) continuous transition of the rod axis s, (b) transition at a branching point K between three individual rod axes s_1, s_2 and s_3.

3. Program implementation

The method for calculating compliant mechanisms as described above is well suited for the implementation into a graphical user interface due to reoccurring patterns in the mechanism design and solution process. The design of the regarded kinds of compliant mechanisms can be reduced to interconnecting beam elements with a constant cross-section, curved beam elements and beam elements with a flexure hinge contour. Assigning geometric Parameters to each element like lengths and curvature radii allows to create an arbitrary shaped continuous compliant mechanism. The implementation of a branching point offers further design possibilities. Adding boundary conditions and applying forces complements the design process. The presented graphical user interface is developed using the programming language *Python* as described in the following sections.

3.1. Program structure of the Python-based graphical user interface

Because of its accessibility, efficiency, readability and numerous available libraries like *NumPy* and *SciPy* for scientific computing, the realization of the given analytical method is implemented with the free and open-source programming language *Python 3.6*. For the creation of a graphical user interface the free software *Pyside2* for the *Qt* toolkit is applied that includes a vast collection of widgets for building a GUI.

The developed GUI is shown in Fig. 9 on the example of a slider-crank mechanism. The interface is categorized into three main modules that are located on the upper left side of the GUI: the **design** of a compliant mechanism and its analysis under given loads, the conduct of **parametric studies** and the **synthesis** as a target-specific evaluation of the performed parametric studies. On the right of the interface, the current mechanism design is plotted in its undeflected and – after the solution has been calculated – in its deflected state. Below, the parameters of the constructed mechanism are outlined in a table format for one beam or for three beams in case a branched mechanism has been designed. In this table the geometric parameters of each element can be modified to achieve a desired shape of the mechanism. Also, forces in x- and y-direction can be applied to any of the associated elements. Another important aspect is the possibility to change the applied theory for each element individually between pure bending ($theory = 0$), including shear ($theory = 1$) or including lateral contraction ($theory = 2$).

A flow chart of the implemented modules is given in Fig. 10. At first, input parameters for the material of the mechanism as well as the initial position within the coordinate system and boundary conditions for point A^* and point B^* can be defined. A desired compliant mechanism can be created by adding the pre-defined building blocks as needed and adjusting their geometric parameters. Furthermore, a branching point may be added to split up a mechanism into three individual beams interconnected at point K. In such a case the boundary conditions are valid for point A^* at the beginning of beam 1 and point B^* at the end of beam 2. The end of beam 3 is chosen to be a free end in all applications. Forces may be applied to the end point of any of all incorporated elements. The given design under the given loads can be analyzed by pressing the analyze-button. After the analyze-button has been pressed and a solution was found, the resulting displacements, angles and elastic strains are outlined for each individual element on the right of the in- and output table. When parametric studies should be performed, an arbitrary geometric or force parameter of any of the incorporated elements can be chosen within the parametric study module. An interval needs to be specified for the chosen parameter and the study can be performed by pressing the run-button. When all designs are calculated, the results are outlined in an extra table and can be exported to a text file. This allows further processing by other software. After a parametric study has been carried out it may be necessary to find the optimum of the calculated modifications considering a specific design-goal. For this purpose, the synthesis module is provided wherein an objective function may be designed by choosing objectives for any element of any beam and related weighing factors. The optimum of the previously calculated parameter modifications is obtained.

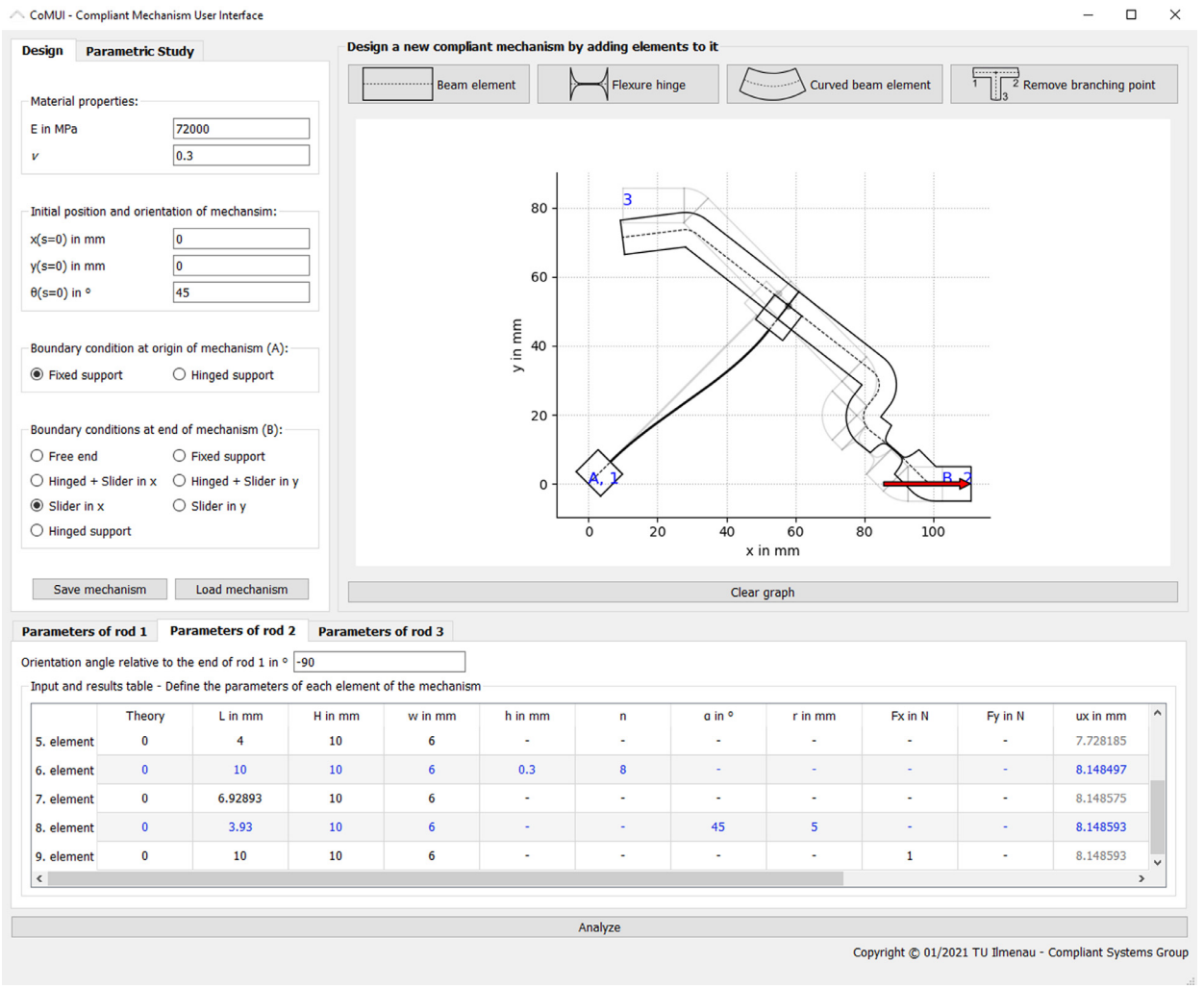

Fig. 9. Screenshot of the developed GUI on the example of a compliant slider-crank mechanism deflected at point B^*.

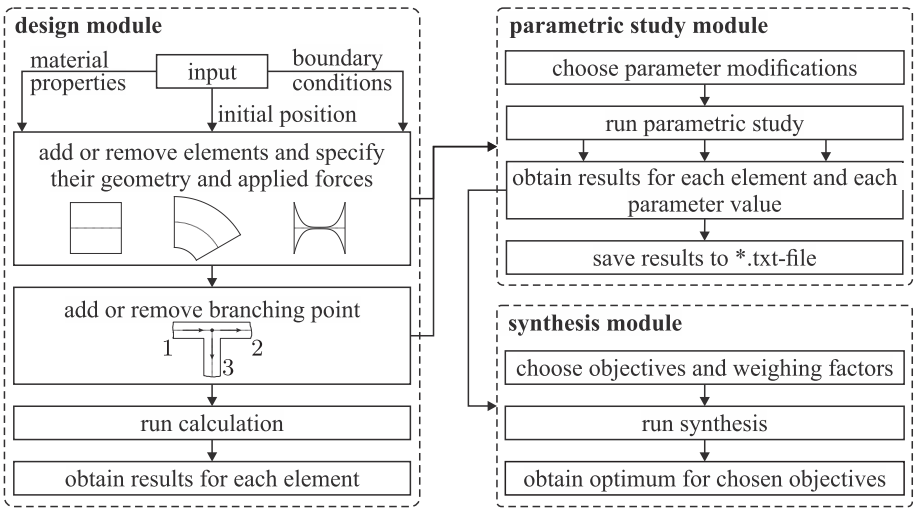

Fig. 10. Structure of the three modules implemented in the given GUI.

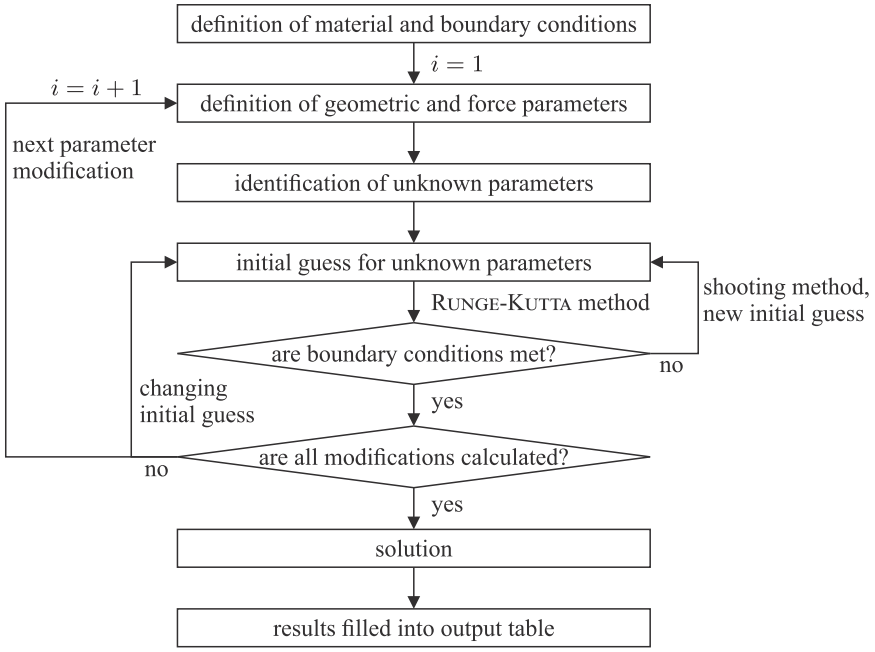

Fig. 11. Flowchart of the solution process for the boundary value problem of a single analysis and parametric studies.

3.2. Mathematical implementation

In the back end of the GUI the element-wise establishment of a mechanism design is interpreted as follows. Originating at the initial position of the coordinate system all elements added to beam 1 are representing a section of the beam axis s_1. The different elements are distinguished according to their curvature-radii and their second moment of inertia I_z that depends on the geometry of an element. Thus, the assembly of individual elements does represent a continuous path of the beam axis s_1 with the according transitions explained in Section 2.6. This single beam represents the model in Fig. 1. Forces at any point along the beam axis and boundary conditions at the ends A^* and B^* complement the model. The boundary conditions at both ends can randomly be combined as long as a statically determinate structure results.

In case a branching point was added to a mechanism design, three self-contained beams result that each are continuous in the same way as described for beam 1. Unlike the case of only one continuous beam, the boundary conditions are defined for the beginning of beam 1 (point A^*) and the end of beam 2 (point B^*). Due to the fact, that the end of beam 3 always represents a free end, another boundary condition results at this location, namely $M_{z3}(s_{3\text{end}}) = 0$. The three beams are interconnected at a branching point K that is located at the end of beam 1. Their orientation relative to the end of beam 1 can be chosen by an orientation angle. As a consequence of the connection point, the initial conditions for beam 2 and beam 3 are available as transition conditions explained in Section 2.6.

Given an arbitrary compliant mechanism design with or without a branching point, it is ensured that the number of boundary and transition conditions matches the number of unknown system parameters. Therefore, the present boundary value problem can be solved numerically for each beam with respect to the given transition and boundary conditions. For this purpose, a combination of a four-step RUNGE-KUTTA method with a shooting method is suitable. Both functions are available within the *SciPy* library for the *Python* programming language. The RUNGE-KUTTA method is applied by the function *RK45* and the shooting method by the function *fsolve* analogously to the *MATLAB*®-functions *ode45* and *fsolve*.

The solution process is shown in Fig. 11. After the material, boundary conditions and geometry have been defined, the unknown system parameters are identified depending on the boundary conditions and, if applicable, transition conditions. The unknown system parameters can be the support reaction forces and moments as well as the moments at the branching point according to Eq. 46. At first, an initial guess for the unknown system parameters is needed within the solution process. Assuming the system parameters are stored in an array called v, an array for the initial conditions may be called v_0. As an initial guess within the software, an array of zeros is considered ($v_0 = 0$). After an initial guess is made, the boundary value problem becomes an initial value problem. Thereby, the differential equations are solved applying the four-step RUNGE-KUTTA-method. Subsequently, the results of this calculation are compared to the boundary conditions. In case the boundary conditions are not met, the initial guess has to be changed. This change is done by the algorithm of the shooting method implemented in the function *fsolve*. Afterwards another cycle of solving the differential equations is done. This process continues until the boundary and transition conditions are met within a specific tolerance. When those are finally met a single analysis is finished and results are obtained and the deformed state of the mechanism is plotted.

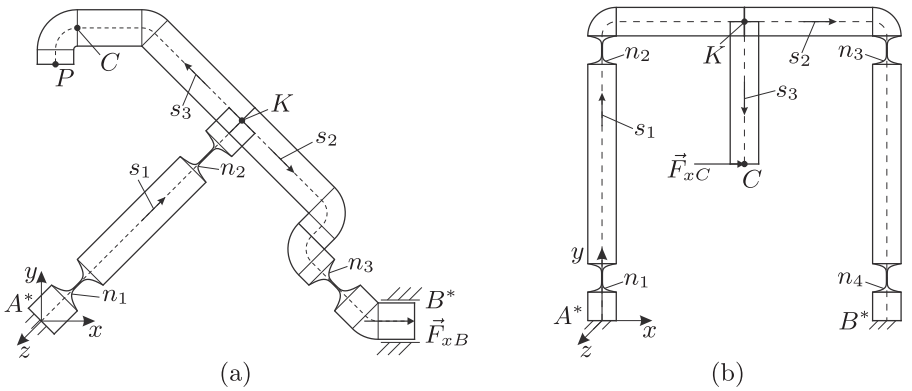

Fig. 12. Example branched mechanisms with power function-based flexure hinges – (a) compliant slider-crank mechanism from [7] $n_1 = 4$, $n_2 = 8$, $n_3 = 4$, (b) compliant parallel four-bar linkage from [30] with $n_{1,\dots,4} = 6$.

When parametric studies are carried out, the next parameter modification has to be calculated. The results for the system parameters v of one calculation can be used as initial conditions for the next modification to speed up the solution process. If i was a counter for the iterations in a parametric study with $i \in \mathbb{N}_1$, the initial guess is called v_{0i} and the related result is called v_i. The first calculation would be done according to Eq. 47.

$$v_{01} = 0. \tag{47}$$

The result of the first iteration will be v_1. The second iteration can be performed with v_{02} using the result of the previous iteration according to the following equation:

$$v_{02} = v_1. \tag{48}$$

For all following iterations the initial guess is generalized to Eq. 49 where the two previous results are used to formulate an initial guess for the next iteration.

$$v_{0i} = v_{i-1} + v_{i-2}, \text{ for } i > 2 \tag{49}$$

This method accelerates the solution process tremendously and also allows an iterative solution if a load case might be too high for a single analysis because of numerical errors occurring. In such a case, the force may be applied step-wise so that a solution can be found for the desired load. Once all parameter modifications are calculated, the results are filled into the in- and output table at the bottom of the GUI (Fig. 9) and, in case of a parametric study, within the according module.

Afterwards, the synthesis module may be used. In this module an objective function can be created to evaluate the parametric study with respect to the desired optimum. In the given GUI, the objective function is minimized according to Eq. 50.

$$f_0 = \min\left(\sum_{j=1}^{k} W_j \tilde{q}_j - \sum_{m=k+1}^{p} W_m \tilde{q}_m\right) \tag{50}$$

A total of p objectives can be selected. The number of objectives to be minimized is k while $p - k$ objectives may be maximized. The objectives $\tilde{q}_j$ and $\tilde{q}_m$ can represent the displacements u_x, u_y, the angle θ and the elastic strain $\varepsilon_{\max}$. Those objectives may be selected for any end point of the available elements of a compliant mechanism design. Furthermore, weighing factors W_j and W_m may be applied to emphasize a certain criterion.

Due to different physical values, the objectives are normalized. For the normalization a min-max feature scaling is utilized according to Eq. 51 on the example of q_j based on the minimum and maximum values of the resulting data from the parametric study.

$$\tilde{q}_j = \frac{q_j - \min(q_j)}{\max(q_j) - \min(q_j)} \tag{51}$$

4. Verification and application

Following, compliant mechanism examples are investigated using the given models and the developed software *CoMUI*. First, the results are compared to FEM simulations and measurements from previous investigations ([7], [30]) to verify the implemented analytical model. Afterwards, further mechanism examples are considered for verification and to demonstrate the different modules of the GUI.

Table 2
Verification of the *CoMUI*-results on the example of the compliant slider-crank mechanism from [7].

Method	F_{xB} in N	$\varepsilon_{\max}$ in %	u_{xC} in µm	u_{yC} in µm	$u_{yP} - u_{xP}$ in µm	δ in °
			Results for a deflection of $u_{xB} = 2$ mm:			
3D FEM	0.55	0.18	4.0	2052.7	1927.7	1.640
Measurement	-	-	-	-	1911.7 ± 1.9	1.631
MATLAB	0.56	0.17	3.7	2053.8	1929.1	1.640
CoMUI	0.56	0.17	3.7	2053.8	1929.1	1.640
			Results for a deflection of $u_{xB} = 5$ mm:			
3D FEM	1.52	0.47	20.1	5354.5	4999.6	4.188
Measurement	-	-	-	-	4988.3 ± 7.0	-
MATLAB	1.50	0.42	18.8	5356.7	5002.9	4.189
CoMUI	1.50	0.42	18.8	5356.7	5002.9	4.189

Table 3
Verification of the *CoMUI*-results on the example of the compliant parallel four-bar linkage from [30].

Method	F_{xC} in N	$\varepsilon_{\max}$ in %	$\lvert u_{yC} \rvert$ in µm	Time in s
3D FEM	1.443	0.41	613.6	3309
Measurement	1.363	-	599.5	-
MATLAB	1.367	0.43	613.7	19.9
CoMUI	1.367	0.43	613.8	28.1

4.1. Two compliant mechanisms from previous studies

For a first verification, the results obtained using the analytical model implemented in the *Python*-based GUI, two example compliant mechanisms from previous studies are considered. Concentrated compliance in the form of flexure hinges is used in both mechanisms. The compliant slider-crank mechanism from [7] and the compliant parallel four-bar linkage from [30] are shown in Fig. 12 with the according elements necessary for modeling within the analysis module. In both cases, a branching point K is added so that three beams result. The origin of the first beam is fixed at point A^*. The slider-crank mechanism in Fig. 12 (a) is modeled using a slider in x-direction and is deflected by a force in the same direction at point B^*. In case of the parallel four-bar linkage in Fig. 12 (b) point B^* is fixed and a force in x-direction is applied at the end of the third beam in point C. In both publications the displacement was specified as an input. However, in the first version of the given GUI it was decided that only forces are considered which is why the respective forces are iterated until the desired displacement of ± 10 mm is achieved in the following investigations for both mechanisms.

The results from the previous publication for the compliant slider-crank mecahnism are given in Table 2 including the results obtained with the software *CoMUI*. The resulting force F_{xB} due to the x-displacement, the maximum elastic strain $\varepsilon_{\max}$, the stroke u_{yC}, the straight-line deviation u_{xC}, the linear position change of point P: $u_{yP} - u_{xP}$ and the coupler rotation angle δ are evaluated. For this mechanism example, the coupler rotation angle equals the rotation angle at the end of the third beam. The results are given for the two different input displacements $u_{xB} = 2$ mm and $u_{xB} = 5$ mm.

The results for the compliant parallel four-bar linkage are given in Table 3. In this case, the resulting force F_{xC}, the maximum elastic strain $\varepsilon_{\max}$ the guidance error u_{yC} and the respective calculation times are evaluated. The results are given for an input displacement of $u_{xC} = 10$ mm. However, this example has been calculated using a total of 21 load steps.

It can be seen that the *Python*-based results are in very good correlation with the previous calculations. They are almost identical to the MATLAB® results because of the similar algorithms implemented. Compared to the measurement result in case of the complaint parallel four-bar linkage, the resulting force value is in even better correlation than the force value obtained with 3D FEM simulations.

The greatest advantage over 3D FEM simulations is the necessary calculation time which is also given in Table 3. It should be noted, that these times only include the calculation itself once the mechanism has already been designed, boundary conditions have been assigned and, in case of FEM, meshed. In previous investigations based on the analytical model, the establishment of the MATLAB®-models was a time-consuming task, too. Those models were established significantly faster than CAD and FEM models but were still complex. With *CoMUI* this is now much simpler. The design of compliant mechanisms like the examples in Fig. 12 can be done by simply adding elements and changing their geometry in the table format. The creation of such a mechanism is therefore vastly accelerated and can be achieved in a matter of seconds.

4.2. The influence of pure bending, shear and lateral contraction

To investigate the influence of the three different theories (pure bending - $theory = 0$, shear - $theory = 1$, lateral contraction - $theory = 2$), a parametric study is carried out to evaluate the dependency of the force F_y from the parameters $\tilde{H} = \frac{H}{L}$ and $\tilde{w} = \frac{w}{L}$ for all three analytical models. For the parametric studies a single beam with rectangular cross-section as in Fig. 1 is considered. On one hand, only the parameter $\tilde{H}$ is varied in the interval $\tilde{H} = [0.1, 1]$ while $\tilde{w} = 0.1$ remains

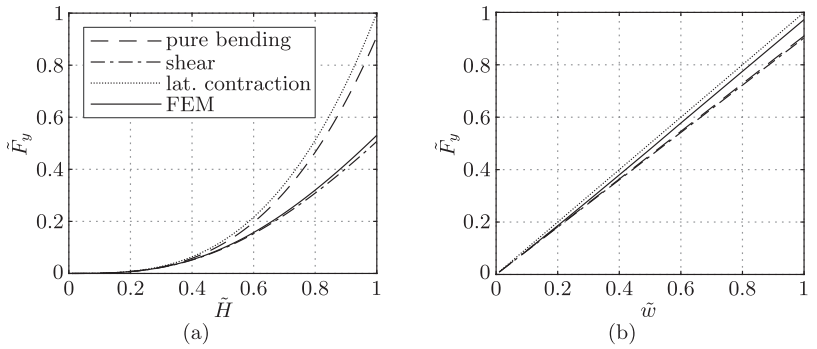

Fig. 13. Resulting force for a beam fixed at one end and deflected by a displacement of $\tilde{u}_y = 0.016$ at the free end while – (a) varying the height $\tilde{H}$, (b) varying the width $\tilde{w}$.

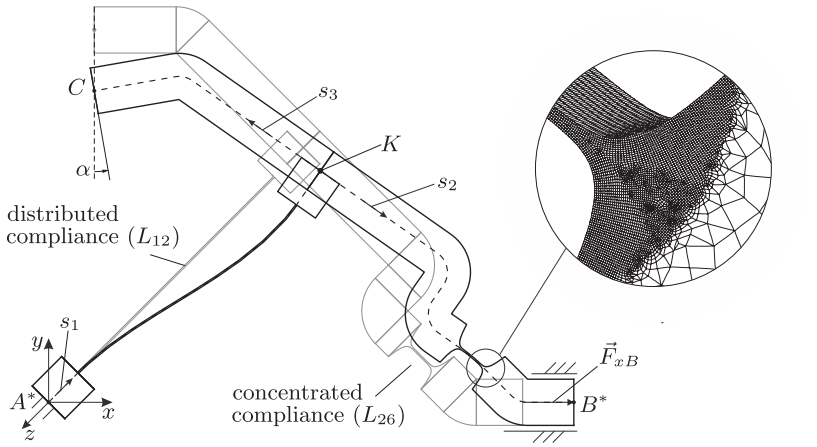

Fig. 14. Undeflected (gray) and deflected (black) state of a compliant slider-crank mechanism with distributed compliance and a flexure hinge with the hinge exponent $n = 8$ and 3D FEM mesh details.

constant. On the other hand, the same study is performed by varying $\tilde{w}$ in the interval $\tilde{w} = [0.1, 1]$ while $\tilde{H} = 0.1$ remains constant. For comparison, the study is also performed in the form of a 3D FEM simulation using *Solid186* hexahedral elements. The total number of elements for each parameter variation remains constant by specifying the number of divisions over the length, the height and the width of the beam. The number of divisions has been evaluated until the results converged.

First, the analytical model for pure bending ($theory = 0$) is taken into account. The beams are deflected by a displacement in y-direction of $\tilde{u}_y = 0.016$ which equals a deflection angle of $\theta = 10°$. The same displacement is used as an input for the other two analytical models. In case of the FEM simulations, the beams are deflected by a force on the face of the free end until the same deflection of $\tilde{u}_y = 0.016$ is reached. All resulting force values of the parametric study are shown in Fig. 13.

In Fig. 13 (a) the parameter $\tilde{H}$ has been varied and in Fig. 13 (b) the parameter $\tilde{w}$. The force values are normalized to $\tilde{F}_y$ using the maximum resulting force.

In Fig. 13 (a) it becomes clear that the influence of shear increases with higher ratios $\tilde{H}$. The analytical model including shear ($theory = 1$) coincides well with the FEM simulation results while the other two analytical models exceed a deviation of 5% for ratios of $\tilde{H} \geq 0.3$.

Similar facts can be concluded from the results in Fig. 13 (b). The higher the ratio of $\tilde{w}$ is, the greater the effect of lateral contraction becomes. The analytical model including lateral contraction ($theory = 2$) yields better agreement with FEM simulation results compared to both other analytical models for $\tilde{w} \geq 0.48$. Before this ratio, $theory = 2$ yields higher deviations than both other analytical models.

4.3. Slider-crank mechanism with distributed compliance

In the next example, the point-guidance slider-crank mechanism in Fig. 12 (a) is modified so that distributed compliance is present in the first beam by replacing both flexure hinges and the connection in between them by a single thin element as depicted in Fig. 14.

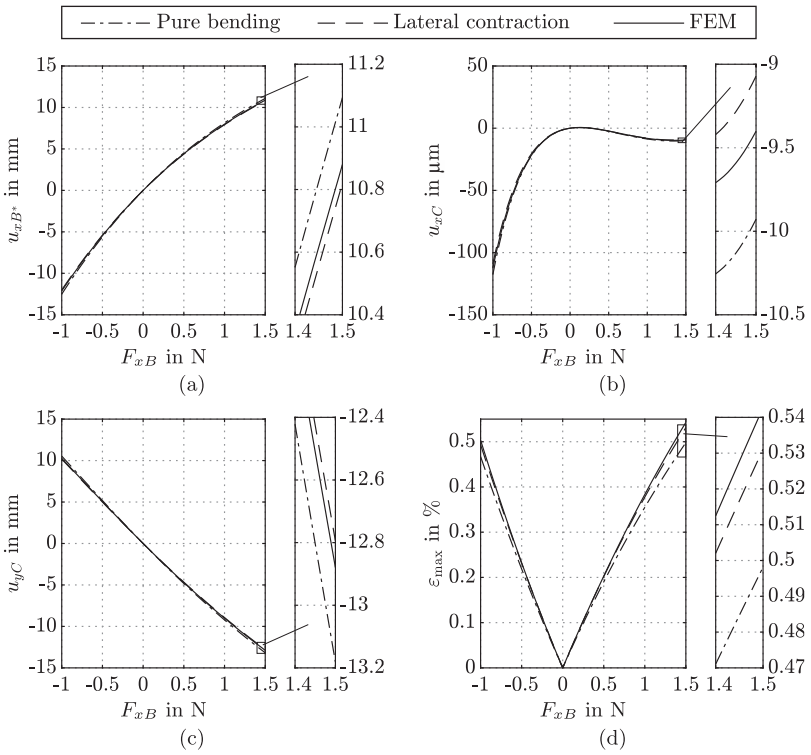

Fig. 15. Analytical and FEM results for the slider-crank mechanism with distributed compliance loaded at point B^* with an input force F_{xB} =-1 N to 1.5 N – (a) deflection u_{xB^*}, (b) deflection u_{xC}, (c) deflection u_{yC}, (d) maximum elastic strain $\varepsilon_{\max}$.

The mechanism is deflected by an input force $\vec{F}_{xB}$ in point B^* while point A^* remains fixed. In the following investigation the input force is varied in an interval of -1 N to 1.5 N in steps of 0.01 N. The displacement of point B^* in x-direction, the displacement of point C in x- and y-direction as well as the resulting maximum elastic strain $\varepsilon_{\max}$ are evaluated by means of the analytical model and 3D FEM simulations.

The overall width of the mechanism is chosen as $w = 6$ mm. The element with distributed compliance (second element of the first beam) is modeled as an element with constant cross-section with a length of $L_{12} = 60$ mm and a height of $H = 0.3$ mm. The flexure hinge (sixth element of the second beam) on the other hand is modeled as an eighth order power function-based contour with a minimum height of $h = 0.3$ mm and a contour length of $L_{26} = 10$ mm. Concerning the material, the aluminum alloy EN AW 7075 with a YOUNG's modulus of 72 GPa is considered.

First, the analytical calculation of the compliant slider-crank mechanism is performed assuming pure bending. However, when considering the width to length ratios of both compliant elements that experience the largest deformation, a ratio of $\tilde{w} = 0.1$ results at the element with distributed compliance and $\tilde{w} = 0.6$ at the flexure hinge. With regard to the results of Section 4.2, it is advisable to apply the effects of lateral contraction ($theory = 2$) within the flexure hinge only, while assuming pure bending in all other elements. Hence, in addition to the results obtained with pure bending a second analytical calculation is carried out applying lateral contraction in the flexure hinge.

The results are compared to 3D FEM simulations because it is assumed that those are closest to reality due to a plane strain state. The mechanism is meshed using *Solid186* hexahedral elements with a size of 1 mm globally and refined at the element with distributed compliance and the flexure hinge with an element size of 0.05 mm as shown in Fig. 14. The element size was studied until the results converged.

The results of the calculations over the input force are given in Fig. 15 for all three scenarios. From the diagrams it becomes clear that for all considered points, the deviations between the two different analytical theories and the 3D FEM simulations are in good correlation. However, when magnifying the results, the consideration of lateral contraction within the flexure hinge provides a significantly better correlation with the 3D FEM results.

The absolute values and the relative deviations of both analytical models from the 3D FEM results for the force F_{xB} = 1.5 N are given in Table 4. In addition to the aforementioned displacements and maximum elastic strain the angle α has been evaluated, too. For each result the deviation from 3D FEM simulations could drastically be reduced by applying lateral contraction within the flexure hinge only.

Table 4
Results for the force $F_{xB} = 1.5$ N and deviations of the calculation with pure bending and the calculation assuming lateral contraction at the flexure hinge from 3D FEM simulations.

Method	u_{xB} in mm	u_{xC} in µm	u_{yC} in mm	ε_{max} in %	α in °
3D FEM	10.886	–9.4	–12.887	0.54	9.72
CoMUI (*theory* = 0 at L_{26})	11.093	–9.9	–13.182	0.50	9.88
↰ deviation to 3D FEM	1.90%	5.32%	2.29%	–7.41%	1.65%
CoMUI (*theory* = 2 at L_{26})	10.820	–9.1	–12.795	0.53	9.61
↰ deviation to 3D FEM	–0.61%	–3.19%	–0.71%	–1.85%	–1.13%

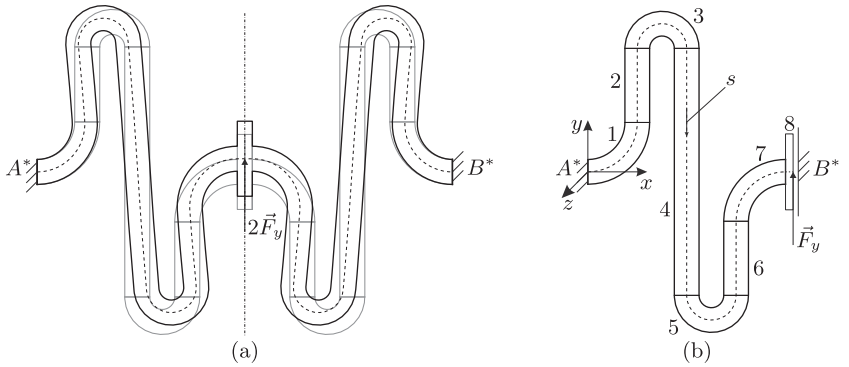

Fig. 16. Compliant guidance mechanism – (a) complete symmetric model in its undeflected (gray) and deflected (black) state, (b) half model consisting of 8 sections.

4.4. An exemplary synthesis task for a compliant guidance mechanism

Next, the compliant guidance mechanism with distributed compliance in Fig. 16 (a) is considered. Because of the distributed compliance, pure bending ($theory = 0$) is assumed. The mechanism is fixed at both ends A^* and B^* and is deflected by a force $\vec{F}_y$ in its geometric center. Because of the axial symmetry, the model can be simplified into a half model depicted in Fig. 16 (b). Therein, the boundary condition at point B^* is replaced by a slider in y-direction to simulate the same motion behavior as the complete model. This boundary condition can be selected within the input module of the GUI. Also, only half of the original force is considered. In that case, the compliant mechanism design is created by using a composition of eight curved and straight beam elements starting at the origin in point A^*. Using the analysis module, it can be shown that the displacement in y direction at the point of force application is the same for both cases (a) and (b).

With respect to a certain synthesis task for the given example, the largest possible y-displacement under a given load could be of interest. This is demonstrated by changing the length L_4 of the fourth element along the beam axis s in the interval from 2 mm to 10 mm in steps of 0.1 mm. This interval equals a total of 81 necessary calculations. The height and width of the elements one to seven is $H_{1,\dots,7} = 1$ mm while the height of the eighth element is $H_8 = 3$ mm. The width is constant along s by $w_{1,\dots,8} = 1$ mm. The lengths of the straight beam elements are chosen as follows: $L_2 = L_6 = 3$ mm, $L_8 = 0.3$ mm. The curvature angles of the first and last curved beam elements are $\alpha_1 = 90°$ and $\alpha_7 = -90°$ whith curvature radii of $r_1 = r_7 = 2$ mm. The curved elements three and five are modeled with $\alpha_3 = -180°$, $\alpha_5 = 180°$ and $r_3 = r_5 = 1$ mm. As a material, the aluminum alloy ENAW7075 with a YOUNG's modulus of 72 GPa is assumed. A constant force of $F_y = 50$ N is applied at the end of the eighth element.

First, the mechanism design has to be done by adding elements and adjusting their geometry. In order to find the optimum length L_4 within the given interval for the desired maximization of u_{y8}, a parametric study is carried out within the corresponding module. After setting up the parametric study and pressing the run-button, all modifications are calculated. The results are given in the embedded table and can be exported for any element of the mechanism. In this case, the data is exported for the eighth element.

The characteristic curve $u_{y8}(L_4)$ for the given example is evaluated using the exported data and plotted in Fig. 17. Due to the non-linear characteristics, it is non-trivial to find the optimum in advance. In fact, the synthesis module can be applied after the parametric study has been performed.

Once a parametric study has been carried out, the resulting data concerning displacements, angles and maximum elastic strains are obtained for each element of each individual beam and can be stored for further processing. It may then be conceivable that an optimal solution for a special application will be sought. In that case, the synthesis module can be applied. On the example of the guidance mechanism of Fig. 16 and the resulting data of the parametric study, the objective of the synthesis is to maximize the y-displacement of the eighth element. For this purpose, the objective function f_0 is

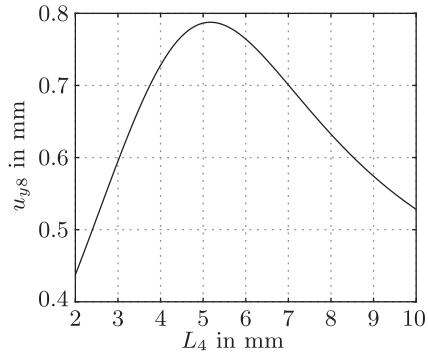

Fig. 17. Characteristic curve of the displacement of the eighth element in dependency of the length of the fourth element.

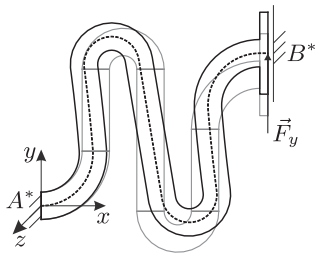

Fig. 18. Optimum geometry for the compliant guidance mechanism with respect to the maximum y-displacement at point B^*.

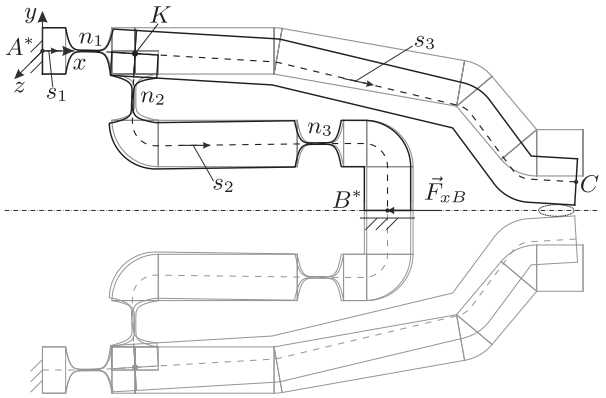

Fig. 19. Undeflected (gray) and deflected (black) state of a compliant gripper mechanism with power function-based flexure hinge contours of sixth order and detailed mesh in case of FEM simulations.

selected and reduced to Eq. 52 as the maximization of u_{y8}:

$$f_0 = \min(-\tilde{u}_{y8}). \tag{52}$$

The result of the synthesis module yields the parameter $L_4 = 5.2$ mm as the optimum length of the fourth element for the given objective to maximize the y-displacement of the eighth element. The result coincides with the data in Fig. 17. The optimum geometry is demonstrated in Fig. 18.

In summary, the design of the example guidance mechanism has been very intuitive by adding elements to the path of the beam axis s and changing their geometry accordingly. It is easily possible to select the necessary boundary conditions for the given compliant mechanism. A parametric study can be performed by specifying one parameter (L_4 in the example) and choosing an interval for it. It should be mentioned, that the total of 81 calculations takes less than 40 seconds on an average PC to highlight the efficiency. To find the optimum length L_4 with respect to the highest y-displacement at the end point under a constant force, the synthesis module has been used to select the according objective.

Table 5
CoMUI and FEM simulation results for the compliant gripper mechanism with pure bending considered in all elements of the mechanism.

Method	u_{xB} in mm	u_{xK} in mm	u_{yK} in mm	u_{xC} in mm	u_{yC} in mm
3D FEM	–0.484	–0.014	–0.550	–1.402	–5.943
CoMUI ($theory = 0$)	–0.512	–0.016	–0.582	–1.493	-6.285
↰ deviation from 3D FEM	5.79%	14.29%	5.82%	6.49%	5.75%

4.5. Compliant gripper mechanism

Another application with a symmetrical design is the compliant gripper mechanism shown in Fig. 19. Because of its symmetry, the mechanism can be split in half and modeled as a mechanism with only one fixed end in point A^*, one branching point K and a slider in x-direction at point B^*.

The graphical user interface can be used for the design of the mechanism and for studying the dependency of the output displacement u_C from an input force $\vec{F}_{xB}$. With this dependency, the gripping force for different sized objects can be determined. In the example, all three flexure hinges are modeled as sixth order power function-based contours with a minimum height of $h = 0.3$ mm and a contour length of $L = 10$ mm. Again, the width of the mechanism was chosen as $w = 6$ mm which yields a ratio of $\tilde{w} = 0.6$ in the center of the flexure hinges. As in previous examples, the aluminum alloy EN AW 7075 with a YOUNG's modulus of 72 GPa is considered. Assuming the force $F_{xB} = -4$ N, the resulting displacements of the points B^*, K and C are given in Table 5 considering pure bending in the case of *CoMUI*. The results are compared to 3D FEM simulations with the same specifications as in Section 4.3.

Based on the results it becomes clear that the analytical model is less stiff compared to 3D FEM and larger displacements occur. This leads to deviations of around 6%. The deviation of more than 14% in case of u_{xK} results because of the low absolute values.

According to Fig. 13 and the observations made in Table 4, the given ratio $\tilde{w} = 0.6$ in the center of the flexure hinges may be the reason for the resulting deviations compared to 3D FEM simulations when pure bending is considered. Better accordance may be achieved by applying the model that includes the effects of lateral contraction. To verify this, the cal-

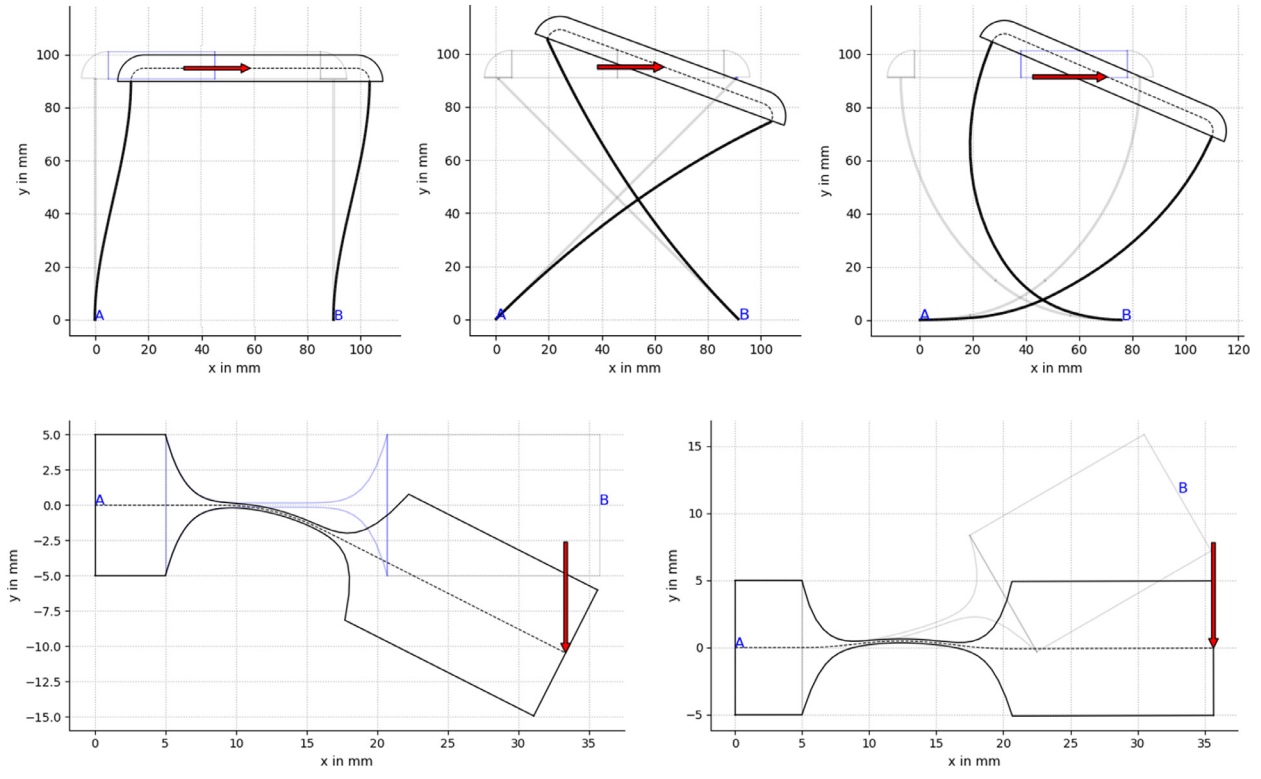

Fig. 20. Further mechanism examples that have been calculated using *CoMUI* – top: different compliant mechanisms, bottom: flexure hinge without and with initial curvature.

Table 6
CoMUI and FEM simulation results for the compliant gripper mechanism with lateral contraction applied within the flexure hinge n_2 only.

Method	u_{xB} in mm	u_{xK} in mm	u_{yK} in mm	u_{xC} in mm	u_{yC} in mm
3D FEM	–0.484	–0.014	–0.550	–1.402	–5.943
CoMUI ($theory = 2$ at n_2)	–0.479	–0.014	–0.546	-1.392	-5.903
↳deviation from 3D FEM	–1.03%	N/A	–0.73%	–0.71%	–0.67%

culation is repeated by applying lateral contraction ($theory = 2$) at the flexure hinge with the highest deformation, which appears to be the hinge n_2. All other sections are still calculated using pure bending ($theory = 0$).

The results from this investigation are given in Table 6. It can be seen that the deviations between the analytical calculation and the FEM simulation are drastically reduced when lateral contraction is considered at the flexure hinge with the highest deformation. The same behavior was observed for different mechanisms, too and needs further investigation in future research.

4.6. Special application cases

Apart from the examples given, a number of different mechanisms can be investigated with the help of the software. Some special application cases that have been calculated using *CoMUI* are shown in Fig. 20.

One specialty that should be mentioned is that each beam of a mechanism which incorporates crossed beams is considered independent as shown in the upper center of Fig. 20. This can be useful in the design of cross-axis flexure hinges (e.g. [28]). A connection between different beams is only realized when a branching point is introduced. Another possibility is the consideration of initially curved flexure hinges as shown on the bottom right of Fig. 20.

5. Conclusions

With this contribution, the authors presented the theories for shear and lateral contraction in a unified form with the theory for large deflections of rod-like structures. By describing compliant mechanisms as continua it has been shown that the theories can be chosen individually for specific sections that may present various aspect ratios. The given model is applicable for compliant mechanisms including branched links, varying cross-sections, curvatures or material properties. Large deflections are considered and the boundary value problem can be solved numerically within a short time frame. Building on those theories, an intuitive and practical *Python*-based graphical user interface for the analysis and synthesis of compliant mechanisms has been developed. With the use of three different building blocks – beam elements with constant cross-section, curved beam elements and flexure hinges – a compliant mechanism can easily be designed. By adjusting their geometry, the compliance of each element can be influenced in a targeted manner. This allows good accessibility for an engineer with little experience in the compliant mechanism analysis and synthesis. The range of applications was significantly increased by implementing a branching point. A multitude of possible boundary conditions allows a wide applicability to known mechanism examples. External loads can be applied, the deformed state of the mechanism is calculated and important elasto-kinematic properties like flexure hinge angles, displacements and elastic strains are evaluated. Furthermore, the possibility to carry out parametric studies allows to identify parameter dependencies and to find an optimal solution for a given task. The greatest advantage of the given GUI is the fast establishment of a mechanism design and the equally fast analysis which can speed up the solution process immensely. The analytical solution has been verified by means of FEM simulations and measurements. It could be shown that the consideration of lateral contraction at the flexure hinge with the greatest deformation reduces deviations compared to FEM simulations for large width to length ratios. Those findings will be subject to future research. To better understand the functionality of the proposed tool, a demonstration video is provided as supplementary material. A download link to the software can be provided upon request to the corresponding author.

Declaration of Competing Interest

The authors declare that they have no known competing financial interests or personal relationships that could have appeared to influence the work reported in this paper.

Acknowledgments

The authors would like to gratefully acknowledge the support of the German Research Foundation (DFG) under grant number ZE 714/10-2.

Supplementary material

Supplementary material associated with this article can be found, in the online version, at 10.1016/j.mechmachtheory.2021.104397

References

[1] Handbook of Compliant Mechanisms, L.L. Howell, S.P. Magleby, B.M. Olsen (Eds.), Wiley, Chichester, 2013, doi:10.1002/9781118516485.
[2] L. Zentner, S. Linß, Compliant systems: Mechanics of elastically deformable mechanisms, actuators and sensors, De Gruyter, Berlin, 2019.
[3] N. Lobontiu, M. Cullin, In-plane elastic response of two-segment circular-axis symmetric notch flexure hinges: the right circular design, Precis. Eng. 37 (3) (2013) 542–555, doi:10.1016/j.precisioneng.2012.12.007.
[4] J.M. Paros, L. Weisbord, How to design flexure hinges, Machine design 25 (11) (1965) 151–156.
[5] N. Lobontiu, J.S.N. Paine, E. Garcia, M. Goldfarb, Corner-Filleted flexure hinges, J. Mech. Des. 123 (3) (2001) 346–352, doi:10.1115/1.1372190.
[6] S.T. Smith, V.G. Badami, J.S. Dale, Y. Xu, Elliptical flexure hinges, Rev. Sci. Instrum. 68 (3) (1997) 1474–1483, doi:10.1063/1.1147635.
[7] S. Linß, P. Gräser, S. Henning, F. Harfensteller, R. Theska, L. Zentner, Synthesis Method for Compliant Mechanisms of High-Precision and Large-Stroke by Use of Individually Shaped Power Function Flexure Hinges, in: T. Uhl (Ed.), Advances in Mechanism and Machine Science, Mechanisms and Machine Science, 73, Springer International Publishing, Cham, 2019, pp. 1569–1578, doi:10.1007/978-3-030-20131-9_155.
[8] R. Friedrich, R. Lammering, T. Heurich, Nonlinear modeling of compliant mechanisms incorporating circular flexure hinges with finite beam elements, Precis. Eng. 42 (2015) 73–79, doi:10.1016/j.precisioneng.2015.04.001.
[9] P. Bilancia, S.P. Smith, G. Berselli, S.P. Magleby, L.L. Howell, Zero torque compliant mechanisms employing pre-buckled beams, J. Mech. Des. 142 (11) (2020), doi:10.1115/1.4046810.
[10] M.A. Torres Melgarejo, M. Darnieder, S. Linß, L. Zentner, T. Fröhlich, R. Theska, On modeling the bending stiffness of thin semi-Circular flexure hinges for precision applications, Actuators 7 (4) (2018) 86, doi:10.3390/act7040086.
[11] S. Li, G. Hao, W.M. Wright, Design and modelling of an anti-buckling compliant universal joint with a compact configuration, Mech Mach Theory 156 (2021) 104162, doi:10.1016/j.mechmachtheory.2020.104162.
[12] L.F. Campanile, R. Jähne, A. Hasse, Exact analysis of the bending of wide beams by a modified elastica approach, Proceedings of the Institution of Mechanical Engineers, Part C: Journal of Mechanical Engineering Science 225 (11) (2011) 2759–2764, doi:10.1177/0954406211417753.
[13] M. Ling, L.L. Howell, J. Cao, G. Chen, Kinetostatic and dynamic modeling of flexure-based compliant mechanisms: A Survey, Appl Mech Rev 72 (3) (2020), doi:10.1115/1.4045679.
[14] P. Bilancia, G. Berselli, An overview of procedures and tools for designing nonstandard beam-Based compliant mechanisms, Comput.-Aided Des. 134 (2021) 103001, doi:10.1016/j.cad.2021.103001.
[15] N. Lobontiu, Compliant mechanisms: Design of flexure hinges, CRC Press, Boca Raton, 2003.
[16] Y.M. Tseytlin, Notch flexure hinges: an effective theory, Rev. Sci. Instrum. 73 (9) (2002) 3363–3368, doi:10.1063/1.1499761.
[17] L. Yuanqiang, L. Wangyu, Analysis of the displacement of distributed compliant parallel-guiding mechanism considering parasitic rotation and deflection on the guiding plate, Mech Mach Theory 80 (2014) 151–165, doi:10.1016/j.mechmachtheory.2014.06.005.
[18] V. Megaro, J. Zehnder, M. Bächer, S. Coros, M. Gross, B. Thomaszewski, A computational design tool for compliant mechanisms, ACM Trans Graph 36 (4) (2017) 1–12, doi:10.1145/3072959.3073636.
[19] M.L. Culpepper, S. Kim, A Framework and Design Sythesis Tool Used to Generate, Evaluate and Optimize Compliant Mechanism Concepts for Research and Education Activities, in: Volume 2: 28th Biennial Mechanisms and Robotics Conference, Parts A and B, ASMEDC, 2004, pp. 1583–1588, doi:10.1115/DETC2004-57606.
[20] V.K. Venkiteswaran, H.-J. Su, A parameter optimization framework for determining the pseudo-rigid-body model of cantilever-beams, Precis. Eng. 40 (2015) 46–54, doi:10.1016/j.precisioneng.2014.10.002.
[21] O.A. Turkkan, H.-J. Su, DAS-2D: A concept design tool for compliant mechanisms, Mech. Sci. 7 (2) (2016) 135–148, doi:10.5194/ms-7-135-2016.
[22] F. Ma, G. Chen, Influence of non-ideal fixed-end constraints on kinetostatic behaviors of compliant bistable mechanisms, Mech Mach Theory 133 (2019) 267–277, doi:10.1016/j.mechmachtheory.2018.11.008.
[23] L. Yuanqiang, L. Wangyu, W. Lei, Analysis of the displacement of lumped compliant parallel-guiding mechanism considering parasitic rotation and deflection on the guiding plate and rigid beams, Mech Mach Theory 91 (2015) 50–68, doi:10.1016/j.mechmachtheory.2015.04.007.
[24] N. Lobontiu, Compliance-based matrix method for modeling the quasi-staticresponse of planar serial flexure-hinge mechanisms, Precis. Eng. 38 (3) (2014) 639–650, doi:10.1016/j.precisioneng.2014.02.014.
[25] Z. Xiangzhou, L. Yougao, D. Zhiyong, B. Hongzan, Statics of rotational 3-UPU parallel mechanisms based on principle of virtual work, in: IEEE International Conference on Robotics and Biomimetics, 2007, IEEE Service Center, Piscataway, NJ, 2007, pp. 1954–1959, doi:10.1109/ROBIO.2007.4522466.
[26] Q.T. Aten, S.A. Zirbel, B.D. Jensen, L.L. Howell, A numerical method for position analysis of compliant mechanisms with more degrees of freedom than inputs, J. Mech. Des. 133 (6) (2011), doi:10.1115/1.4004016.
[27] K. Wu, G. Hao, Design and nonlinear modeling of a novel planar compliant parallelogram mechanism with general tensural-compresural beams, Mech Mach Theory (2020) 103950, doi:10.1016/j.mechmachtheory.2020.103950.
[28] P. Bilancia, G. Berselli, S. Magleby, L. Howell, On the modeling of a contact-aided cross-axis flexural pivot, Mech Mach Theory 143 (2020) 103618, doi:10.1016/j.mechmachtheory.2019.103618.
[29] G. Chen, F. Ma, G. Hao, W. Zhu, Modeling large deflections of initially curved beams in compliant mechanisms using chained beam-constraint-model, in: Proceedings of the ASME International Design Engineering Technical Conferences and Computers and Information in Engineering Conference – 2018, American Society of Mechanical Engineers, New York, N.Y., 2018, doi:10.1115/DETC2018-85515.
[30] S. Henning, S. Linß, P. Gräser, R. Theska, L. Zentner, Non-linear analytical modeling of planar compliant mechanisms, Mech Mach Theory 155 (2020) 104067, doi:10.1016/j.mechmachtheory.2020.104067.
[31] A. van Beek, Advanced engineering design: Lifetime performance and reliability, ed. 2009, TU, Delft, 2009.
[32] I. Ivanov, Methodical development of a parallel kinematic positioning system based on monolithic structures with flexure hinges, RWTH Aachen, Aachen, 2016 Dissertation.
[33] S. Henning, S. Linß, L. Zentner, DetasFLEX – A computational design tool for the analysis of various notch flexure hinges based on non-linear modeling, Mech. Sci. 9 (2) (2018) 389–404, doi:10.5194/ms-9-389-2018.
[34] P. Bilancia, G. Berselli, L. Bruzzone, P. Fanghella, A CAD/CAE integration framework for analyzing and designing spatial compliant mechanisms via pseudo-rigid-body methods, Robot Comput Integr Manuf 56 (2019) 287–302, doi:10.1016/j.rcim.2018.07.015.
[35] A. Milojević, N.D. Pavlović, M. Milošević, M. Tomić, New Software for Synthesis of Compliant Mechanisms, in: Proceedings of The 2nd International Conference Mechanical Engineering in XXI Century, Niš, Serbia, 2013.
[36] K. Liu, A. Tovar, An efficient 3D topology optimization code written in matlab, Struct. Multidiscipl. Optim. (Structural and Multidisciplinary Optimization) 50 (6) (2014) 1175–1196, doi:10.1007/s00158-014-1107-x.
[37] M.P. Koster, Constructieprincipes voor het nauwkeurig bewegen en positioneren, vijfde druk, vijfde oplage, ThiemeMeulenhoff, Amersfoort, 2008.
[38] V.K. Venkiteswaran, O.A. Turkkan, H.-J. Su, Speeding up topology optimization of compliant mechanisms with a pseudorigid-Body model, J Mech Robot 9 (4) (2017), doi:10.1115/1.4035992.
[39] B. Zhu, X. Zhang, H. Zhang, J. Liang, H. Zang, H. Li, R. Wang, Design of compliant mechanisms using continuum topology optimization: a review, Mech Mach Theory 143 (2020) 103622, doi:10.1016/j.mechmachtheory.2019.103622.
[40] The art of flexure mechanism design, F. Cosandier, S. Henein, M. Richard, L. Rubbert (Eds.), EFPL Press and CRC Press Taylor & Francis Group, Lausanne and Boca Raton, Fl., 2017.
[41] S.P. Timoshenko, LXVI. On the correction for shear of the differential equation for transverse vibrations of prismatic bars, The London, Edinburgh, and Dublin Philosophical Magazine and Journal of Science 41 (245) (1921) 744–746, doi:10.1080/14786442108636264.
[42] J. Dankert, H. Dankert, Technische mechanik: Statik, festigkeitslehre, kinematik/kinetik, 4. korrigierte und ergänzte auflage, B. G. Teubner Verlag / GWV Fachverlage GmbH Wiesbaden, Wiesbaden, 2006, doi:10.1007/978-3-8351-9083-2.

[43] M. Zichner, Mechanismenelemente mit lokal angepasster Nachgiebigkeit, Technische Universität Dresden, Dresden, 2018 Dissertation.
[44] H. Balke, Einführung in die Technische Mechanik: Festigkeitslehre, Springer-Lehrbuch, 2008.
[45] S. Linß, T. Erbe, L. Zentner, On polynomial flexure hinges for increased deflection and an approach for simplified manufacturing, in: International Federation for the Promotion of Mechanism and Machine Science (Ed.), 13th World Congress in Mechanism and Machine Science, Curran, Red Hook, NY, 2011.